Shuttle Solid Rocket Booster Bolted Field Joint Shape Optimization

Jean-François M. Barthelemy*
NASA Langley Research Center, Hampton, Virginia
Kwan J. Chang†
PRC Kentron, Hampton, Virginia
and
James L. Rogers Jr.‡
NASA Langley Research Center, Hampton, Virginia

A structural optimization procedure is used to determine the shape of an alternate design for the Shuttle's solid rocket booster field joint. In contrast to the tang and clevis design of the existing joint, this design consists of two flanges bolted together. Configurations with 150 studs of $1\frac{1}{8}$ in. diam and 135 studs of $1\frac{3}{16}$ in. diam are considered. Using a nonlinear programming procedure, the joint weight is minimized under constraints on either von Mises or maximum normal stresses, joint opening, and geometry. The procedure solves the design problem by replacing it with a sequence of approximate (convex) subproblems; the pattern of contact between the joint halves is determined every few cycles by a nonlinear displacement analysis. The minimum weight design has 135 studs of $1\frac{3}{16}$ in. diam and is designed under constraints on normal stresses. It weighs 1144 lb per joint more than the current tang and clevis design.

Introduction

THE January 28, 1986, Space Shuttle accident is believed to have been caused by a failure of the pressure seal in the aft field joint of the right solid rocket booster. The first recommendation of the presidential commission[1] established to examine the circumstances of the accident was a field joint redesign, possibly even the introduction of a totally new joint design. Several different concepts have been considered to modify or replace the current tang and clevis design (see Ref. 2, for example). One of the concepts developed at the NASA Langley Research Center involves a bolted flange joint that is expected to be more predictable and provide better sealing than the current design at the expense of requiring new case segment forgings.[3-5] The joint is depicted in Fig. 1. The end flanges of two consecutive booster segments are bolted together by studs. The studs are recessed to minimize interferences with the airstream, and a cork insulation is included to further smooth out the flow over the joint. The continuity of the longitudial stresses across the joint is insured by the presence of gussets that divert some of the shell stresses and also reduce the bending in the shell. The studs are pretensioned and sealing is provided by one c-ring and one o-ring. The joint material includes the following steels[3]: D6AC for the shell, MP35N for the studs, and Inconel 718 for the nuts. Initial analyses revealed that the baseline bolted joint was heavier than the current design while still opening under load and having areas of very high stresses. It was decided to try and remedy these problems using the tools of optimization (nonlinear programming).

Received March 9, 1987; presented as Paper 87-0702 at the AIAA/ASME/ASCE/AHS 28th Structures, Structural Dynamics, and Materials Conference, Monterey, CA, April 6-8, 1987; revision received Nov. 10, 1987.

*Aerospace Engineer, Interdisciplinary Research Office, Structures Directorate. Member AIAA.
†Project Structures Engineer, Advanced Computer Methods.
‡Aerospace Technologist, Interdisciplinary Research Office, Structures Directorate.

This problem belongs to the class of structural shape optimal design. The joint model considered is a three-dimensional solid. A recent survey of the structural optimization literature by Haftka and Grandhi[6] reveals little experience with this type of model. This is because two major components of the shape optimization process, automatic finite-element mesh generation and shape sensitivity analysis, are not yet developed enough for fully three-dimensional models. Automatic mesh generation is necessary because, as the initial shape of the solid is changed in the optimization process, the initial finite-element mesh may become so distorted that it is inadequate and a new mesh must be regenerated, a procedure that is tedious and time consuming if performed manually. Current automated procedures still remain interactive and consume hours of computer time.[7] There are two approaches to calculating analytical shape sensitivity derivatives: 1) taking derivatives of the discretized finite-element equations for the structural response or 2) deriving sensitivity equations directly from the fundamental equations of continuum mechanics. Although both approaches have been developed theoretically and have been applied with various success to two-dimensional (or axisymmetric) problems, a recent review by Adelman and Haftka[8] reports no example that involves shape sensitivity analysis of three-dimensional solids.

In two applications of three-dimensional shape optimization, Imam[9,10] models the shape of the structure using a series of design elements that distort as the structure geometry changes. Each design element is itself subdivided into a fixed number of finite elements for structural analysis, thereby providing for a simple automated mesh generation capability where a new mesh is generated with each design but the number of finite elements is fixed at the outset. Gross geometrical dimensions are chosen as design variables (up to four). Satisfactory results are reported for simple beams or engine bearing cap models. Sensitivity analysis is performed by finite difference. In another application, Wasserman[11] uses a similar concept of hyperelements to optimize gravity dams, taking coordinates and slopes of the cross section of the dam (up to 20) as design variables. A special-purpose sensitivity analysis procedure is devised based on directly taking derivatives of the discretized finite-element equations.

This paper describes the shape optimization of a bolted solid rocket booster field joint concept. The joint weight is mini-

mized under constraints that limit the stresses in the model and that also ensure that the gap between two consecutive booster segments remains closed. The optimization model includes six geometrical variables as well as one variable controlling the pretension in the studs. As for the design element and hyperelement approaches described above, the finite-element mesh adapts to changes in geometry, but the number of finite elements is fixed. The model behavior is nonlinear because the pattern of contact between the two joint halves is unknown at the outset. Optimization is performed by replacing the initial nonlinear nonconvex design problem with a sequence of approximate convex subproblems solved with the usable-feasible direction method. Strong initial constraint violation is overcome by using a constraint relaxation technique. Gradients are obtained by finite difference. The details of the finite-element model and analysis used to determine stresses and displacements are given first. Then the optimization approach is presented. A few words follow about computer implementation of the procedure, and optimization results are given.

Finite-Element Model and Analysis

The geometry of a nominal joint model is shown in Fig. 2. The joint behavior is assumed to be symmetric with respect to 1) the interface between two consecutive booster segments, 2) a plane through the booster axis and a stud axis, and 3) a plane through the booster axis bisecting the angle between two consecutive stud axes. The length of the model is 50 in., a distance at which the bending in the shell caused by the joint stiffness has become negligible, and the shell stresses match those predicted by membrane theory for internal pressure loading within 1%.

The finite-element model selected is depicted in Fig. 3. It has 410 four-, six-, and eight-node solid finite elements based on an assumed stress field[12] formulation. The applied loads correspond to an internal pressure of 1000 psi. This is slightly more than the pressure observed anywhere in the booster during ignition. These loads include 1) internal pressure on the inner shell nodes (1000 psi), 2) resultant of pressure effect in axial direction on model top nodes (36,406 lb/in.), and 3) contact forces due to compression of the sealing rings (which are not modeled); these are applied at the first inner row of nodal points on the bottom of the flange (500 lb/in.). Also, the pretension in the stud is modeled as a temperature drop. Although the final design of this joint should include more load cases such as nonsymmetric ones, this case is felt to be representative of the loads encountered by the booster; further, it has been used in other studies[2–5] and thereby provides a good basis for comparison.

The boundary conditions applied to the model enforce radial displacement for the nodes on planes passing through the booster axis and the edges of the model. The nodes at the top of the model are free. The boundary conditions for the bottom of the model flange are variable and depend on how the flange bottom contacts the foundation. Where there is contact between joint halves, the nodes have constrained axial displacement; otherwise, the nodes are free. Finally, the stud and nut are monolithic, and the nodes on the bottom of the nut and the corresponding ones on the top of the flange are constrained to the same displacements. Also, the nodes on the bottom of the stud have no axial displacement. After imposition of the boundary conditions, the model has approximately 2200 degrees of freedom.

The structural analysis of the model is nonlinear because the pattern of contact between the two joint halves is unknown. In other words, it must be determined whether the axial degrees of freedom for the nodes on the bottom of the model are free or fixed. This is done in an iterative fashion. An initial pattern is assumed. Then a conventional linear finite-element analysis is conducted. The axial nodal displacements and reactions are examined at the bottom of the flange. If a node where contact is assumed shows negative axial reaction, this indicates a tendency toward joint opening and the axial degree of freedom is freed. If a node where no contact is assumed shows negative axial displacement, this indicates a tendency toward joint closing, and the axial degree of freedom is fixed. A new displacement analysis is performed, and the process is continued until convergence. For this example where the contact surface contains 17 nodes, these nonlinear analyses required up to 5 cycles.

Optimization Model and Procedure

The variables of the problem are given in Fig. 2. Variable X_1 determines the radial position of the stud axis and, therefore, controls the opening of the joint. If the stud axis is well outside of the shell walls, the tensions developed in the shell tend to

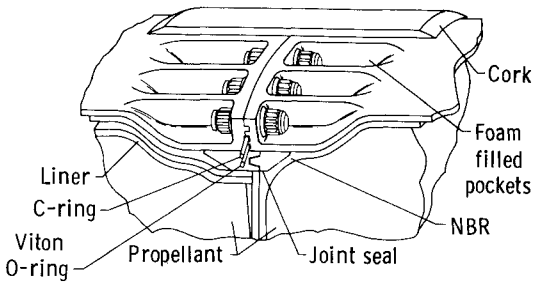

Fig. 1 Proposed bolted joint configuration (from Ref. 3).

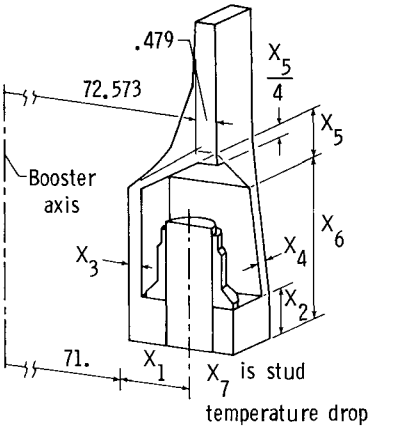

Fig. 2 Joint optimization model.

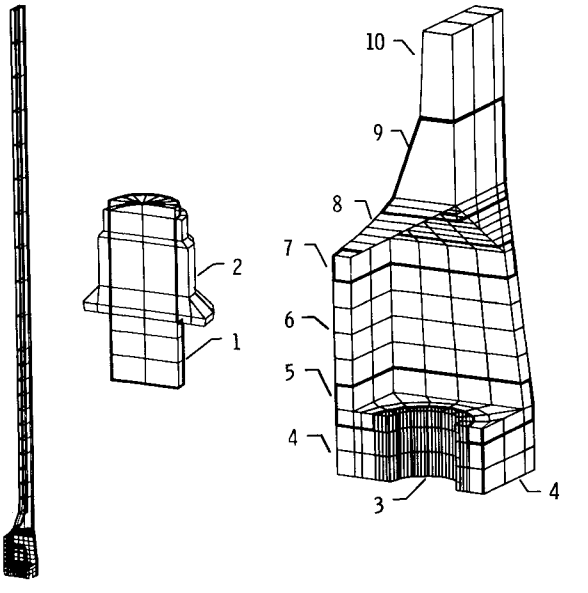

Fig. 3 Joint finite-element model, element groups definition.

open the inside of the joint (see Fig. 4). If the stud axis is well inside of the shell, most of those tensile stresses are carried by the gusset, and the joint opens on the outside. The latter behavior is definitely more desirable than the former since the sealing rings are located toward the inside of the joint. An additional variable X_7 specifies a drop in temperature for the stud thereby simulating stud prestressing; this variable is also very important in controlling the joint opening. The optimization problem objective function is the model weight. The effect of changes in stud diameter were studied by considering two specific designs, one with 150 studs of $1\frac{1}{8}$ in. diam and a second with 135 studs of $1\frac{3}{16}$ in. diam.

For each element, the analysis gives stress values at each of the nodes. At each node of the model, the stresses are defined as the averages of those predicted for the particular node in each of the elements that are connected to it. During the optimization process, stress constraints limit the average nodal stresses observed in the joint. There is one stress constraint for each element; it is either the von Mises stress criterion or a limit on the maximum (in absolute value) normal stress observed in the element (in the remainder of the text, these are referred to as the von Mises stress constraint or the normal stress constraint). There are thus 410 stress constraints. In order to facilitate tracking these constraints, the elements are assembled in 10 groups as depicted in Fig. 3.

Figure 5 depicts the node pattern on the bottom of the flange; it is divided into three areas. The innermost area is where contact is enforced between two consecutive booster segments in order to ensure positive sealing and prevent exhaust of hot gases. The contact is controlled by constraining the sign of the reactions for the two innermost rows of nodes on the flange. At these eight nodes, the reactions are constrained to remain compressive. The flange outermost area is where the two segments are free to contact or not depending on the loading conditions. In the remaining area, essentially under the nut-bearing surface, contact is prevented by the presence of a milled recess in the flange; this leaves the innermost and outermost flange areas for contact between the two joint halves. Preliminary sensitivity studies have shown that this facilitates joint closing.

Three geometrical constraints are added; two guarantee that the stud and the nut can be inserted in the joint, and the third one prevents excessive compression of the finite-element mesh in the straight shell area immediately next to the joint. The design problem includes 421 constraints. The gradients required for optimization are obtained by backward finite difference (assuming that the contact pattern at the base of the flange is not affected by the perturbation in the variables).

Optimization is conducted by replacing the initial nonlinear, nonconvex, and implicit problem with a sequence of nonlinear but convex and explicit subproblems. The mathematical details of the subproblem formulation are given in the Appendix. At the starting point of each cycle, a new subproblem is constructed. The objective function and constraints are approximated by convex approximations based on first-order analysis information. The total number of constraints is reduced from 421 to 14 by associating one cumulative constraint with each of the 10 element groups and one with the 8 reaction constraints. This cumulative constraint is a conservative envelope function that preserves the convexity of the approximations. To accommodate starting points with strongly violated constraints, a constraint relaxation procedure is added. Each convex subproblem is solved using a usable-feasible direction procedure.

Typical optimization starting points considered in this study have most constraints violated. This can cause difficulties for the usable-feasible direction optimization procedure used. The design procedure is, therefore, conducted in three steps. A starting design is chosen that satisfies the three geometrical constraints. In the first step, only the stud stress constraint and the joint closure constraint are retained in the problem. Both of those constraints are relaxed, and optimization is conducted to satisfy them. In the second step, the relaxation is removed from

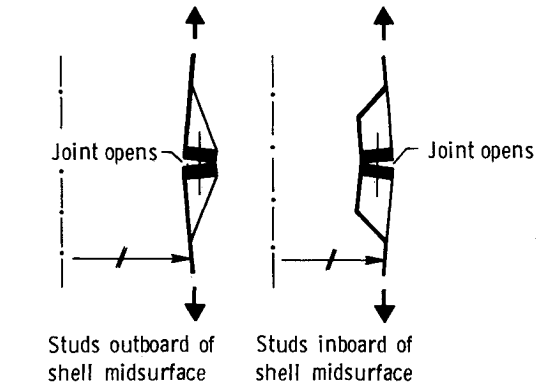

Fig. 4 Joint opening pattern depends on radial position of stud.

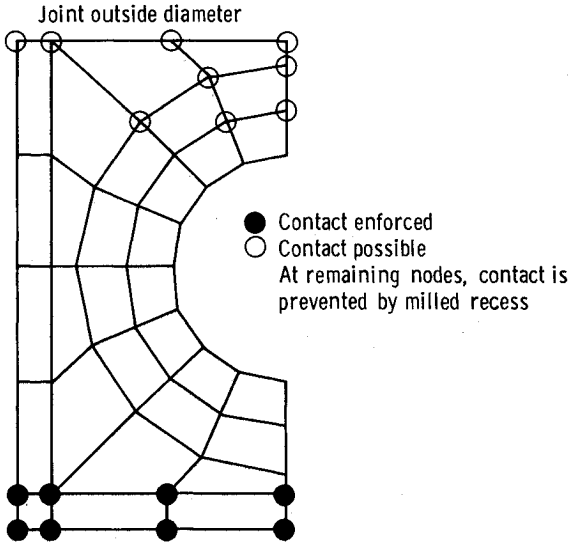

Fig. 5 Flange bottom contact pattern.

the stud stress and the joint closure constraints; the remaining stress constraints are added and relaxed, and optimization is continued until all the constraints are satisfied or critical. In the third step, relaxation is removed from all constraints involved, and weight minimization is continued to convergence. During optimization, the pattern of contact between joint halves is continuously changing as the design evolves. To reduce computational time, nonlinear displacement analyses are only performed every few (typically five) cycles; otherwise, the flange bottom boundary conditions are assumed to be unchanged from the previous cycle, and only linear finite-element analysis is performed.

Computer Implementation

The procedure described above is implemented using the existing PROSSS[13] system as core software. Structural analysis is performed with the EAL[12] finite-element program, and optimization is carried out with the CONMIN[14] code. The solid model of the joint and the initial finite-element discretization are generated with the I-DEAS[15] package. As optimization changes the initial model, a special-purpose FORTRAN code has been developed that generates updated nodal coordinates. Intermediate and final structural analysis results are reviewed using the postprocessing capabilities of the I-DEAS package.

The procedure executes on DEC VAXstation II computers with 6 MB of main memory and 71 MB hard disks. Because sensitivity analysis uses finite difference, eight complete structural analyses must be conducted before constructing an approximate subproblem and continuing with optimization. These analyses are conducted in parallel on four workstations simultaneously. As analysis time strongly dominates the total

computational cycle time, this distributed mode of execution enables a speed-up factor of about four yielding a complete optimization cycle in slightly less than one hour of clock time. This is described in detail in Ref. 16.

Most of the procedure is implemented in single precision (32-bit) except for the structural analysis stiffness matrix assembly and decomposition, which use double precision. Comparison of analysis output with results obtained entirely with 60-bit arithmetics indicates that 3–4 digits are reliable for displacements and reactions. Although this type of accuracy is sufficient for analysis results, difficulties arise when derivatives of response quantities are to be obtained by finite difference. Experimentation indicates that finite-difference step sizes of up to 20% of the variables considered are required to minimize the effect of round-off errors. Clearly, significant truncation errors must be anticipated, and decreased approximate subproblem fidelity must be expected. Therefore, all subproblems are solved with move limits that restrict the range of the design variables during approximate subproblem optimization. These move limits are initially prescribed to be 10% of the initial design variables and are reduced to 5% if approximation accuracy is felt to impede convergence.

Results

Two design studies are described in this section; they correspond to two different configurations of studs with approximately the same total stud cross-sectional area and total nut-bearing area. The first configuration has 150 studs of $1\frac{1}{8}$ in. diam for a total 149 in.^{2} of stud cross-sectional area and 495 in.^{2} of stud-bearing area; the second configuration has 135 studs of $1\frac{3}{16}$ in. diam for a total of 150 in.^{2} of cross-sectional area and 500 in.^{2} of nut-bearing area. It is expected that the 135 stud design will enable the use of a wider gusset and thereby result in a more effective transmission of the axial loads. In each study, two designs are generated. The first design has constraints placed on the von Mises stresses in the structure. For each material, the allowable von Mises stress is taken as the lowest of the ultimate tensile allowable stress divided by a 1.4 safety factor or the yield allowable stress divided by a 1.25 factor.[3] For the shell, the stud, and the nut, this corresponds to 139.0, 191.0, and 172.0 ksi, respectively. The second design is similar to the first, except that the stress constraints are placed on the maximum normal stresses. The allowable stresses are unchanged for the stud or the nut. However, the normal stresses in the shell are allowed to reach 155.0 ksi, a value representative of stress levels observed in the current design under the same load case.[2] For all the design cases, optimization is conducted until complete convergence. The weighting factor γ for the constraint violation term in the objective function (see Appendix) is varied between 10^4 and 10^9; this results in the final constraint violation being 1% or less ($0.00 \leq \omega - 1 \leq 0.01$).

In both studies, the stress constraints for the areas immediately around the hole and where the joint transitions to nominal shell (groups 3 and 9, Fig. 3) are not included in the optimization process. Both of those areas are prone to stress concentrations. The hole is in the flange which, acting as a ring stiffener on a pressure vessel, is in tension. Also, the apex of the joint pocket, where consecutive gussets merge into the nominal shell, actually creates a notch in the shell at a point where it is in tension itself. It is unreasonable to drive the joint design by the presence of these localized high-stress areas. Indeed, these stress concentrations are unavoidable. Any reduction in peak stresses requires reduction of the stress levels from which the concentrations rise and would lead to prohibitive flange and shell thicknesses. Hence, some yielding must be tolerated in these restricted areas, provided the shell material is ductile. This, in turn, is likely to smooth out the stress concentrations. Also, this difficulty may be somewhat reduced by careful local design. Plastic analyses must be performed to substantiate these points.

A comparison of the various designs is given in Table 1. Examination of these results reveals that the von Mises stress constraint is significantly more conservative than the maximum normal stress constraint. Indeed, the latter constraint ignores shear stresses although these contribute to the transfer of loads

Table 1 Comparison of final designs

Number of studs	150	150	135	135
Stud diameter, in.	$1\frac{1}{8}$	$1\frac{1}{8}$	$1\frac{3}{16}$	$1\frac{3}{16}$
Constrained stress	von Mises	max normal	von Mises	max normal
Weight, lb[a]	2674.0	1974.0	277.0	1918.0
Constraint violation[b]	0.000	0.010	0.000	0.007
X_1, in.	1.23	1.16	1.18	1.25
X_2, in.	1.75	1.18	1.98	1.73
X_3, in.	1.06	0.704	0.927	0.374
X_4, in.	0.347	0.356	0.417	0.448
X_5, in.	1.50	1.70	1.32	1.13
X_6, in.	4.12	3.56	4.49	4.22
X_7, °F[c]	4.79	8.22	4.75	8.18
Active constraints[d]				
Stress in groups[e]	5,6,7,10	1,2,5,6,7,10	5,(6),(7),10	1,2,5,6,7,(8),10
Joint closure	*y*	*y*	*y*	*y*
Stud insertion	*y*	*y*	*y*	*y*
Nut insertion	*y*	*y*	(*y*)	*y*
Maximum stress values				
Family 3, ksi	160.0	224.0	162.0	217.0
Family 9, ksi	136.0	151.0	149.0	184.0
Maximum displacements				
Inner diam, mil	0.01	0.00	0.02	0.01
Outer diam, mil	0.46	1.23	0.60	0.00
Stud load, kips[f]	109.0	168.0	122.0	197.0

[a]Weight is excess weight over straight shell for both halves of one field joint. The initial tang and clevis design weighs 774 lb more than a straight shell.[3]

[b]Value is $\omega - 1$ (see Appendix). For example, for a stress constraint, a value of 0.01 indicates that the stress exceeds its allowable by 1%.

[c]Based on a linear thermal expansion coefficient of 0.001 in./°F.

[d]*y* or a number *i* ($0 \leq i \leq 10$) indicates an active constraint; (*y*) or (*i*) indicates an almost active constraint ($0 \leq g \leq 0.05$).

[e]For this particular design, constraints 6 and 7 are redundant.

[f]If stressed axially to its allowable (191 ksi), a $1\frac{1}{8}$ in. stud carries 190 kips while a $1\frac{3}{16}$ in. stud carries 212 kips.

between the flange and the gusset. Further, it also ignores such unfavorable combination of normal stresses with compression and tension acting in orthogonal directions. As a result, there are marked differences between designs that have different stress constraints but the same stud configuration. In contrast, designs with the same stress constraint but with different stud configurations are similar, pointing to the fact that the design is probably driven more by the total stud cross-sectional area and nut-bearing area than by the specific combination of stud diameter and number of studs. The results indicate that this specific bolted design can carry a penalty of about 1144 to 2003 lb per joint over the current tang and clevis design, depending on the assumption regarding the stress being constrained. Trajectory calculations[3] indicate that there is a penalty of about 0.100 to 0.125 lb of payload per pound of structural weight added to each booster. Therefore, the results shown here would imply a payload loss of between 114 and 250 lb per joint.

Note that although the designs under von Mises stress constraints have no constraint violation ($\omega - 1 = 0$), both designs under maximum normal stress constraint have some minor violation ($\omega - 1 > 0$). This is true despite attempts at solving the relaxed problem with γ coefficients [see Eq. (A7) of Appendix] of up to 10^9. As explained in the Appendix, this indicates that there is no feasible design for the maximum normal stress constraints; however, the violations are so small that they are of no significance.

The active and nearly active constraints include the joint closure and the nut and stud insertion constraints for all designs. The stress constraints for the top layer of elements in the flange (constraint 5) and for the nominal shell (constraint 10) are always active. Constraint 5 is dominated by tensile stresses in the flange and compressive bearing stresses due to the nut. Constraint 10 involves axial tension due to internal pressure and hoop tension due to internal pressure as well as the concentration at the apex of the joint pocket. The stress constraints for element groups 6 and 7 are dominated by axial tensile stresses in the gusset; they are nearly active for the designs under von Mises stress constraints and active for those under normal stress constraints. Finally, the stud (element group 1) and the nut (element group 2) are constrained to their allowables for the designs under maximum normal stress constraints.

Variable X_1, the stud axis position, affects the gap closure as well as bending stresses in the shell; the final position of the stud axis is about 0.6 in. inboard of the nominal shell midplane. Variable X_7, the stud preload, affects the joint closure as well as the bearing stress developed in the top layer of the flange. The preload selection by the procedure does not depend on the stud configuration in these examples but, rather, on the stress constraint hypothesis retained. The general tension in the flange and the compression due to the nut result in an unfavorable von Mises stress so that considerably less preload is allowed under the von Mises stress constraint than under the maximum normal stress constraint. Variable X_2 affects both the joint closure by changing the bending stiffness of the flange and the hoop stresses in the flange. Variable X_2 is larger under the von Mises stress constraint than under the maximum normal stress constraint because the stud preload is lower. The difference is larger for the 150 studs configuration than for the one with 135 studs, probably because there is more distance between studs in the latter configuration and therefore more stiffness is needed to keep the joint closed. Variables X_3 and X_4 control the amount of material available to carry the axial loads from the joint plane to the nominal shell. The nut insertion constraint essentially acts as an upper bound to the gusset thickness, and the thicker gusset available in the 135 stud configuration favorably reduces the shell thickness. Generally, going from von Mises stress to normal stress constraints is also favorable. Finally, variable X_6 controls the pocket height and is directly affected by the stud insertion constraint; it essentially equals X_2 plus the minimum clearance needed for the stud.

In the areas where the stresses were not constrained, the designs show stresses which, although higher than the allowables, remain lower than some of the stresses observed in the current tang and clevis design.[2] The displacements observed on the inside of the joint are extremely small and testify to the efficiency of the joint closure constraint used. At the same time, the displacements at the outside of the joint are relatively small themselves, which indicates that satisfying the stress constraints results in a joint having a relatively high stiffness. Finally, the integrated load on the studs is always significantly lower than the allowable value determined by assuming pure tension loading to the stud allowable stress value. This is partly because the stud is loaded not only in tension but also in bending. For the designs with constraints on the maximum normal stress, the stud stress constraint is active. It is not the case for the design with constraints on the von Mises stress constraints, probably because that would result in bearing stresses on the upper surface of the flange that are too high.

Convergence took up to 30 cycles for each of the four examples discussed. Convergence was sometimes relatively slow; occasionally (in less than 10% of the cases run) is was even impossible, and optimization had to be restarted with a different starting point. These occasional difficulties with convergence can be partially attributed to the relatively tight (10%, sometimes 5%) move limits used. Also, the often conservative convex approximations can be a contributing factor, as reported in Refs. 17 and 18. A typical convergence history is given in Fig. 6 for the 135 studs configuration under von Mises stress constraints. A relatively smooth convergence is obtained in 14 cycles. Optimization is started under displacement and stud stress constraints only. In the first two cycles, the displacement constraint is satisfied by moving the stud inward (decreasing X_1) and by decreasing the shell thickness (X_3) and, therefore, its stiffness. The remaining stress constraints are then added, and the stud moves outward approximately to its initial position while the shell thickness increases significantly to decrease the bending stresses. In general, the stud preload (X_7) decreases steadily to reduce the bearing stresses. At the same time, the flange thickness (X_2) increases to supply the stiffness necessary to keep the joint closed and to limit the flange hoop stresses. As explained above, the pocket height (X_6) generally follows the changes in flange thickness. Also, the gusset width (X_4) is determined by the nut insertion constraint and, therefore, generally follows the stud radial position. Indeed, the further the radial stud position, the larger the circumference available to place the nuts and, as the nut number is fixed, the larger the maximum width available for the gusset.

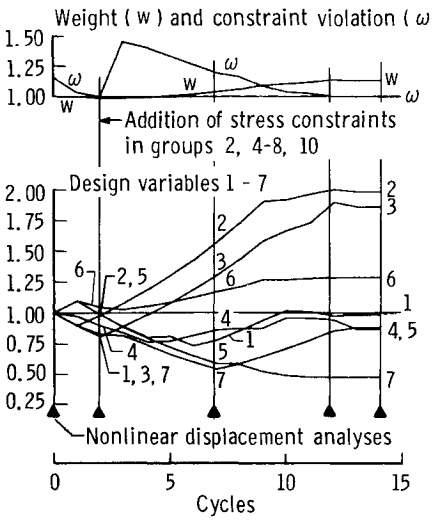

Fig. 6 Convergence history, 135 studs, $1\frac{3}{16}$ in. diam von Mises stress constraints.

A history of the axial displacements in the plane of the joint is given in Fig. 7 for the 135 stud configuration. The 150 stud configuration exhibits the same trends. For this particular example, the initial design has a joint closure constraint nearly satisfied, and therefore no displacement appears at the constrained nodes. As shown in Fig. 6, it takes two cycles to fully satisfy the joint closure constraint on the inside of the joint, while the displacements tend to increase on the outside of the joint where contact is not required. Enforcement of the von Mises stress constraints results in a very significant stiffening of the flange. The same is true to a lesser extent when the maximum normal stress constraints are enforced. In the area of the milled recess, the sagging of the flange never exceeds 3 mil and is not a matter of concern. Also, the stiffness of the flange is high enough that there never is contact between the stud and the hole for the final designs.

Finally, Fig. 8 shows an evolution of the von Mises stress patterns for the same 135 stud configuration. The initial design shows high stresses around the hole and on the upper part of the flange; also, stresses are high at the apex of the pocket. After optimization with von Mises stress constraints (allowable is 139 ksi), the high stress areas have been reduced at the expense of significantly increasing the proportions of the joint. After optimization with maximum normal stress constraints (allowable is 155 ksi), slightly higher stresses are observed, particularly at the top of the gusset; however, the joint proportions are reduced, particularly the thickness of the shell.

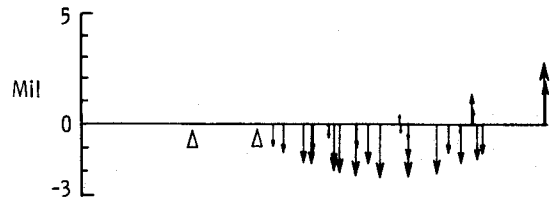

a) Before optimization

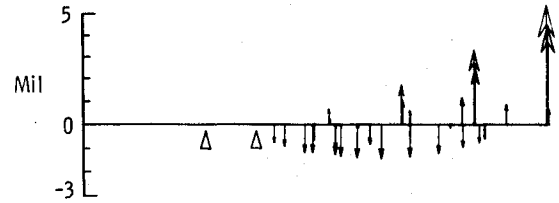

b) After displacement constraints optimization

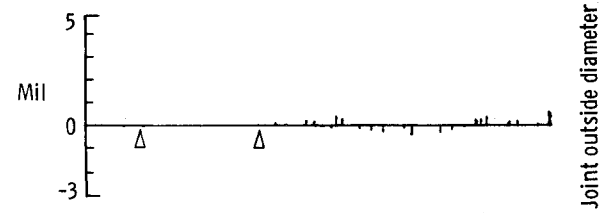

c) After displacement and von Mises stress constraints optimization

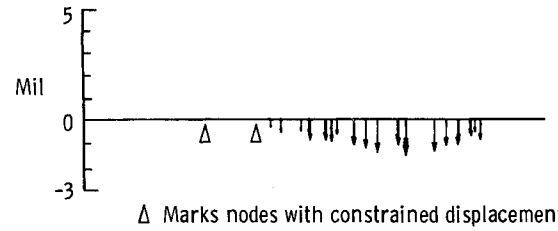

d) After displacement and maximum normal stress constraints optimization

Fig. 7 Flange bottom axial displacements, 135 studs, $1\frac{3}{16}$ in. diam.

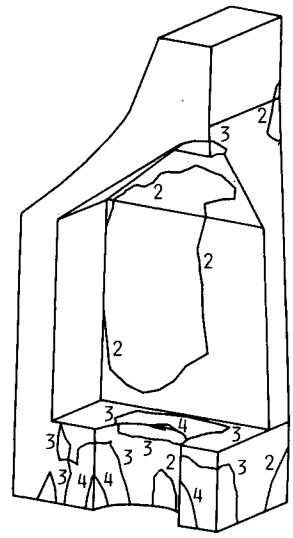

a) Before optimization

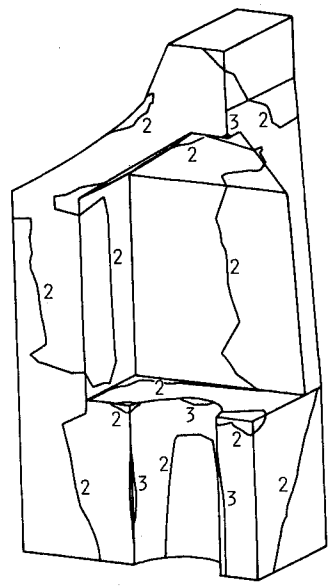

b) After displacement and von Mises stress constraints optimization

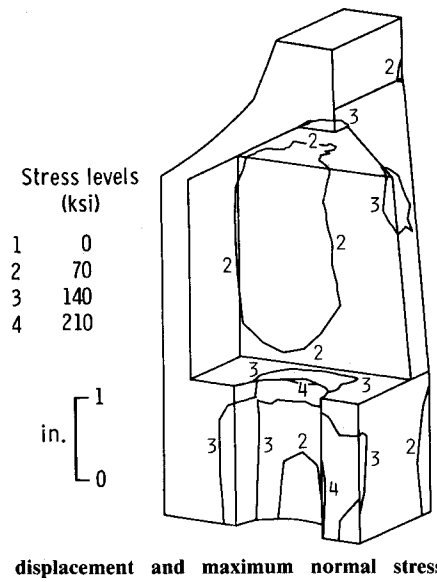

c) After displacement and maximum normal stress constraints optimization

Fig. 8 von Mises stresses in the joint, 135 studs, $1\frac{3}{16}$ in. diam.

Conclusions

A procedure is presented for the structural optimization of the shape of a bolted alternative to the current Space Shuttle solid rocket booster tang and clevis field joint. The design problem is formulated as a minimum weight problem under constraints on stresses, joint opening, and geometry. The joint opening constraint is transformed into a constraint on the sign of the reactions on the faces of the joint. The initial nonconvex, nonlinear, and implicit design problem is replaced by a sequence of nonlinear but convex and explicit problems that are solved in an iterative fashion. A constraint relaxation feature is added to overcome strong initial design infeasibility. The determination of the opening pattern for the joint is found by a nonlinear displacement analysis that is repeated every few cycles in the design process. During optimization, the joint locations in the finite element mesh are modified to reflect the changes in the model shape, but the number of nodes and elements remains fixed. The derivatives required for the optimization process are obtained by finite difference. The procedure generally performs well. Convergence is occasionally slowed down or even stopped. This is related to the use of limited precision software and the resulting need for tight move limits as well as to the use of the often conservative convex approximations.

The procedure is used to optimize designs with two stud configurations under constraints on either von Mises or maximum normal stresses. The loading corresponds to a uniform 1000 psi of internal pressure. The best design obtained uses 135 studs of $1\frac{3}{16}$ in. diam. It weighs 1918 lb or 1144 lb per joint more than the current tang and clevis design. For each joint redesigned in one solid rocket booster, this is estimated to result in a 114 to 143 lb payload penalty. For a given stud configuration, the final design is very sensitive to the stress constraint assumption. On the other hand, the design appears to be relatively insensitive to the stud configuration. The procedure satisfactorily keeps the joint closed and maintains the constrained stresses within their allowables. Two areas are not subjected to stress constraints because they are prone to stress concentration. However, the resulting stresses remain reasonable; they are expected to be further reduced by plastic flow as well as by careful local design, although this must be substantiated by nonlinear plastic analyses.

Appendix: Approximate Subproblem Formulation

The following definitions are used in this appendix.

C_i	= scalar envelope to constraints in vector g_i, Eq. (A6)
$\boldsymbol{g}_i, g_{ij}$	= ith vector of constraints, jth component
h	= scalar function
f	= scalar objective function
n_g	= number of constraint vectors
$\boldsymbol{X}, X_i$	= vector of design variables, ith component
$\boldsymbol{X}^\ell, \boldsymbol{X}^u$	= vectors of lower and upper limits on the variables
α_i	= Eq. (A7)
β	= move limit parameter
γ	= Eq. (A7)
ρ	= Eq. (A6)
$\Sigma_{\ell+}, \Sigma_{\ell-}$	= Eq. (A4)
ω	= relaxation variable
^{o}	= initial value
$\bar{}$	= normalized value
$\tilde{}$	= approximation function

The functional form of the nonlinear programming problem at hand is as follows: find $\boldsymbol{X}$ so that $f(\boldsymbol{X})$ is minimum and

$$\boldsymbol{g}_i(\boldsymbol{X}) \le \boldsymbol{0}, \qquad i = 1, n_g$$
$$\boldsymbol{X}^\ell \le \boldsymbol{X} \le \boldsymbol{X}^u \tag{A1}$$

The constraints are organized in several constraint vectors:

$$\boldsymbol{g}_i^T = (g_{i1}, g_{i2}, \ldots g_{in_i}) \tag{A2}$$

This optimization problem is nonlinear, nonconvex, and implicit. To render optimization cost-effective, the problem is replaced by a sequence of subproblems that are still nonlinear but convex and explicit. The initial subproblem is solved in cycles where the starting point of a cycle is the optimum solution of the subproblem constructed in the previous cycle. Assume that the starting point of the current cycle is $\boldsymbol{X}^o$ (for the sake of clarity, the cycle index is omitted in this discussion). First, the design variable vector is normalized at the starting point:

$$\bar{X}_1 = X_1 / X_1^o \tag{A3}$$

The objective function and the constraints of the problem are then approximated. Assuming that $h(\bar{\boldsymbol{X}})$ is any one of those functions, its approximation is

$$\tilde{h}(\bar{\boldsymbol{X}}) = h(1.) + \Sigma_{\ell+} \frac{\mathrm{d}h(1.)}{\mathrm{d}X_\ell} (\bar{X}_1 - 1.) + \Sigma_{\ell-} \frac{\mathrm{d}h(1.)}{\mathrm{d}X_\ell} X_1^o \left(1. - \frac{1.}{X_1}\right) \tag{A4}$$

where $\Sigma_{\ell+}$ ($\Sigma_{\ell-}$) indicates that the summation is extended to those variables for which the gradient component $\mathrm{d}h(1.)/\mathrm{d}X_\ell$ is positive (negative). For positive design variable values, this approximation is convex[19] and also the most conservative[20] of all those based on first-order information and using terms linear in the variables or their reciprocal. The approximation quality decreases as the design moves away from the initial design $\boldsymbol{X}^o$ so that limits must be introduced to restrict that move; if β is the accepted relative change in the design ($0. < \beta < 1.$),

$$(1. - \beta) \le \bar{\boldsymbol{X}} \le (1. + \beta) \tag{A5}$$

To reduce the number of constraints handled by the optimizer, each vector of approximate constraints $\tilde{\boldsymbol{g}}_i$ is replaced by a scalar constraint C_i:

$$C_i(\bar{\boldsymbol{X}}) = \frac{1}{\rho} \ell n \left\{ \sum_j^{n_i} \exp[\rho \tilde{g}_{ij}(\bar{\boldsymbol{X}})] \right\} \tag{A6}$$

This envelope function is known as the Kreisselmeier-Steinhauser[21] function. It has been shown to be conservative and to preserve the convexity of the approximate subproblem.[18] Parameter ρ is user-supplied and determines how close C_i is to the boundary defined by the $\tilde{g}_{ij}$ constraints.

A final transformation of the subproblem involves the introduction of a selective constraint relaxation capability. A new variable ω is introduced to relax the violated constraints and the new subproblem is then given as follows: find $\bar{\boldsymbol{X}}$, $\bar{\omega}$ so that $\tilde{f}(\bar{\boldsymbol{X}}) + \gamma \bar{f}(1.)\bar{\omega}$ is minimum and

$$C_i(\bar{\boldsymbol{X}}) + \alpha_i(1 - \omega^o \bar{\omega}) \le 0, \qquad i = 1, n_g$$
$$\bar{\boldsymbol{X}}^\ell \le \bar{\boldsymbol{X}} \le \bar{\boldsymbol{X}}^u$$
$$(1. - \beta) \le \bar{\boldsymbol{X}} \le (1. + \beta)$$
$$1./\omega^o \le \bar{\omega} \tag{A7}$$

Parameter α_i is input as either 1. if constraint i must be relaxed or 0. otherwise. The initial value ω^o ($\omega = \bar{\omega}\omega^o$) of the relaxation variable is chosen so that all the constraints are rendered satisfied at the initial design $\boldsymbol{X}^o$ ($\bar{\boldsymbol{X}} = 1.$); it is defined by

$$\omega^o = 1. + \max\{0., \max_{i, \alpha_i \ne 0} [C_i(1.)]\} \tag{A8}$$

Minimization of the new objective function of Eq. (A7) will tend to drive the relaxation variable toward its lower bound. If $\bar{\omega}$ reaches its lower bound, then Eq. (A7) becomes identical to Eq. (A1), except for a constant offset of the objective function.

The non-negative, user-defined parameter γ is chosen so that a predetermined ratio exists at the initial design between the true objective function $\tilde{f}(1.)$ and the penalty term $\gamma\tilde{f}(1.)$. Should the solution of Eq. (A6) still be infeasible for Eq. (A1), it may be necessary to increase that ratio.

Note that if Eq. (A1) does not have a solution, a final value of $\bar{\omega}$ that is greater than $1./\omega^o$ will result. Solving a sequence of subproblems as in Eq. (A7) is a rational approach to finding a design that, in a certain sense, minimizes the violation of the constraints of Eq. (A1).

References

[1]"Report of the Presidential Commission on the Space Shuttle Challenger Accident," Washington, DC, June 6, 1986.

[2]Greene, W. H., Knight, N. F. Jr., and Stockwell, A. E., "Structural Behavior of the Space Shuttle SRB Tang-Clevis Joint," NASA TM 89018, Sept. 1986.

[3]"LaRC Conceptual Design of Solid Rocket Booster In-line Bolted Joint," NASA TM 89046, Dec. 1986.

[4]Lindel, M. C. and Stalnaker, W. A., "Structural Analysis of a Bolted Joint Concept for the Space Shuttle's Solid Rocket Motor Casing," NASA TM 89092, 1987.

[5]Dorsey, J. T., Stein, P. A., and Bush, H. G., "Structural Design of an In-line Bolted Joint for the Space Shuttle Solid Rocket Motor Case Segments," NASA TM 89027, 1987.

[6]Haftka, R. T. and Grandhi, R. V., "Structural Shape Optimization—a Survey," *Computer Methods in Applied Mechanics and Engineering*, Vol. 57, Aug. 1986, pp. 91–106.

[7]Rudd, B. W., "Impacting the Design Process Using Solid Modeling and Automated Finite Element Mesh Generation," *Finite Element Method Modelling and New Applications, Proceedings of 1986 ASME PEP-CIE Conference*, American Society of Mechanical Engineers, New York, July 1986, pp. 5–9.

[8]Adelman, H. M. and Haftka, R. T., "Sensitivity Analysis of Discrete Structural Systems," *AIAA Journal*, Vol. 24, May 1986, pp. 823–832.

[9]Imam, M. H., "Three-Dimensional Shape Optimization," *International Journal for Numerical Methods in Engineering*, Vol. 18, May 1982, pp. 661–673.

[10]Imam, M. H., "Minimum Weight Design of 3-D Solid Components," *Proceedings of the Second International Computer Engineering Conference*, Vol. 3, San Diego, CA, Aug. 1983, pp. 119–126.

[11]Wasserman, K., "Three-Dimensional Shape Optimization of Arch Dams with Prescribed Shape Functions," *Journal of Structural Mechanics*, Vol. 11, No. 4, 1983–84, pp. 465–485.

[12]Whetstone, W. D., *EISI-EAL Engineering Analysis Language Reference Manual—EISI-EAL System Level 312*, Engineering Information System Inc., Aug. 1985.

[13]Rogers, J. L. Jr., Sobieszczanski-Sobieski, J., and Bhat, R. B., "An Implementation of the Programming Structural Synthesis System (PROSSS)," NASA TM 83180, Dec. 1981.

[14]Vanderplaats, G. N., "CONMIN—A FORTRAN Program for Constrained Function Minimization," *User's Manual*, NASA TM X-62282, 1973.

[15]*I-DEAS User's Guide*, Structural Dynamics Research Corp. Milford, OH, 1986.

[16]Rogers, J. L. Jr., Young, K. C., and Barthelemy, J. F. M., "Distributed Computer System Enhances Productivity for SRB Joint Optimization," *Proceedings of the AIAA/ASME/ASCE/AHS 28th Structures, Structural Dynamics, and Materials Conference*, AIAA, New York, April 1987.

[17]Haftka, R. T., "First- and Second-Order Constraint Approximations in Structural Synthesis," *Computational Mechanics* (to be published).

[18]Barthelemy, J. F. M. and Riley, M. F., "An Improved Multilevel Optimization Approach for the Design and Complex Engineering System," *Proceedings of the AIAA/ASME/ASCE/AHS 27th Structures, Structural Dynamics, and Materials Conference*, AIAA, New York, May 1986.

[19]Fleury, C. and Braibant, V., "Structural Optimization, a New Dual Method Using Mixed Variables," Aerospace Laboratory, University of Liege, Belgium, Rept. SA-115, March 1984.

[20]Starnes, J. H. Jr. and Haftka, R. T., "Preliminary Design of Composite Wings for Buckling, Strength, and Displacement Constraints," *Journal of Aircraft*, Vol. 16, Aug. 1979, pp. 564–770.

[21]Kreisselmeier, G. and Steinhauser, R., "Systematic Control Design by Optimizing a Vector Performance Index," *Proceedings of IFAC Symposium on Computer Aided Design of Control Systems*, Zurich, Switzerland, 1979, pp. 113–117.